Turbo-Code Performance with Imperfect Carrier Synchronization

Peter W. Kinman
EECS Department
Case Western Reserve University
10900 Euclid Ave
Cleveland, OH 44106-7071
(216) 368-5550
pwk@eecs.cwru.edu

Shervin Shambayati
Mail Stop 238-420
Jet Propulsion Laboratory
4800 Oak Grove Dr.
Pasadena, CA 91109-8099
(818) 354-1280
shervin.shambayati@jpl.nasa.gov

Layla Tadjpour
Mail Stop 161-260
Jet Propulsion Laboratory
4800 Oak Grove Dr.
Pasadena, CA 91109-8099
(818) 354-7898
layla.tadjpour@jpl.nasa.gov

Jeff B. Berner
Mail Stop 238-737
Jet Propulsion Laboratory
4800 Oak Grove Dr.
Pasadena, CA 91109-8099
(818) 354-3934
jeff.b.berner@jpl.nasa.gov

Abstract—The threshold performance of deep-space telemetry is characterized for four turbo codes. The mathematical models given here are based on simulations that account for imperfect carrier synchronization. The required E_b/N_0 depends on the code, the threshold frame error rate, the bit rate, and the signal-to-noise ratio and bandwidth of the carrier synchronization loop. The performance models are valid for coherent detection of binary phase-shift keyed (BPSK) telemetry. For residual-carrier tracking, these mathematical models are used to calculate the optimum modulation.

1. Introduction

Forward error-correction coding is almost always used in deep-space telemetry. The following four turbo codes are used in this paper: (1784, 1/3), (1784, 1/6), (8920, 1/3) and (8920, 1/6). [1] The first number indicates the code block size and the second number the code rate. The baseline performance of these four turbo codes is defined by [2]

$$\mathrm{FER} = f\left(\left.\frac{E_b}{N_0}\right|_{\mathrm{base}}\right) \tag{1}$$

$$\left.\frac{E_b}{N_0}\right|_{\mathrm{base}} = f^{-1}(\mathrm{FER}). \tag{2}$$

The baseline performance curves are shown in Figure 1.

This paper examines the effect of imperfect carrier tracking on the performance of these four turbo codes. The local oscillator is locked in frequency and phase with the incoming

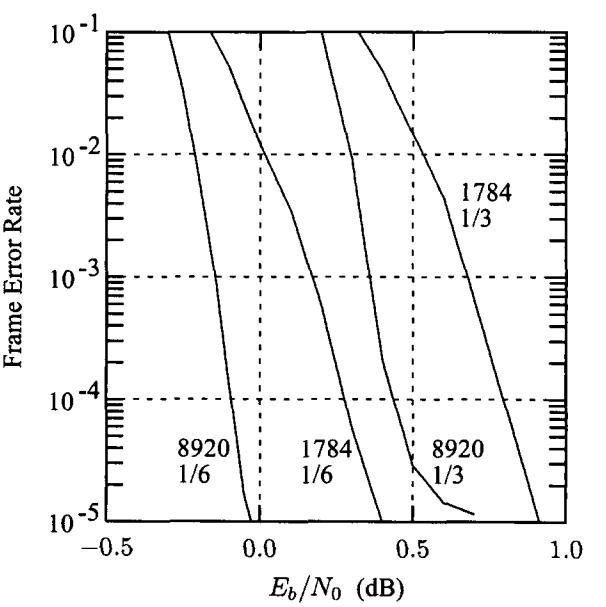

Figure 1: Baseline performance

[1] 0-7803-8155-6/04/$17.00 ©2004 IEEE
[2] IEEEAC paper #1124

telemetry signal by a carrier synchronization circuit. When a residual carrier is present, this circuit is a phase-locked loop that tracks the residual carrier. When the telemetry signal has a suppressed carrier, the synchronization circuit is a Costas loop that extracts frequency and phase information from the data sidebands. In either case, there is a carrier loop that tries to track the phase of the incoming signal but does so imperfectly. There is always noise present in the carrier loop, and this is the main reason that the carrier loop phase error is nonzero.

2. Signal Models

A binary phase-shift keyed (BPSK) telemetry signal with total signal power P_T, carrier (angular) frequency ω and modulation index θ is modeled as

$$\begin{aligned}\sqrt{2P_T}\,\sin(\omega t+\theta d) &= \sqrt{2P_T}\,\cos\theta\cdot\sin(\omega t)\\ &+ \sqrt{2P_T}\,d\sin\theta\cdot\cos(\omega t). \quad (3)\end{aligned}$$

The data are represented in bipolar form by $d = \pm 1$ (an implicit function of time). As shown on the right-hand side of Eq. (3), the signal comprises, in general, two parts: a residual carrier and data sidebands. If $\theta = 90°$, the residual carrier disappears and all of the signal power appears in the data sidebands; this is called a *suppressed carrier*. Both residual-carrier and suppressed-carrier BPSK telemetry are used in deep-space communications. A key telemetry performance parameter is the bit energy to noise spectral density ratio, E_b/N_0. It is given by

$$\frac{E_b}{N_0} = \frac{P_T}{N_0 R}\sin^2\theta, \quad (4)$$

where N_0 is the one-sided noise spectral density and R is the bit rate.

In deep-space communications, a telemetry signal of the form given by Eq. (3) is coherently detected with a local oscillator of the form $\sqrt{2}\cos(\omega t-\phi)$, where ϕ (an implicit function of time) represents the carrier loop phase error. When the data sidebands term, $\sqrt{2P_T}\,d\sin\theta\cdot\cos(\omega t)$, is multiplied by the local oscillator and the product is filtered to remove the double-frequency term, the result is a baseband signal of the form

$$\sqrt{P_T}\,\cos\theta\cdot\sin\phi + \sqrt{2P_T}\,d\sin\theta\cdot\cos\phi.$$

The first term above is typically negligible. (In the case of suppressed carrier, this first term is identically zero.) The second term represents the baseband telemetry signal. It should be noted that the fractional factor $\cos\phi$ degrades the available signal power. It is appropriate to model ϕ as a random process, since it has its origins in noise within the carrier loop. The effect of imperfect carrier tracking is usually modeled like this:

$$\frac{E_b}{N_0}\,(\text{dB}) - L\,(\text{dB}) \geq \left.\frac{E_b}{N_0}\right|_{\text{base}}\,(\text{dB}). \quad (5)$$

$E_b/N_0|_{\text{base}}$ is given by Eq. (2) and L ($L \geq 1$) is the *radio loss*. This statement means that the available E_b/N_0 less the radio loss must exceed the baseline bit energy to noise spectral density ratio for successful telemetry.

3. Radio Loss

Radio loss is modeled here as an interpolation between the LRM and HRM radio losses of Appendix B.

$$L\,(\text{dB}) = a\cdot L_{HRM}\,(\text{dB}) + (1-a)\cdot L_{LRM}\,(\text{dB}) \quad (6)$$

The interpolation factor is given by

$$a = \frac{1}{1+exp\,\{c_1 - c_2\ln(R/B_c)\}}, \quad (7)$$

where B_c is the noise-equivalent carrier loop bandwidth. The coefficients c_1 and c_2 are given by

$$c_1 = \begin{cases} 9.78, & \text{1784-bit block codes}\\ 7.78, & \text{8920-bit block codes,}\end{cases} \quad (8)$$

$$c_2 = \begin{cases} 1.30, & \text{1784-bit block codes}\\ 0.92, & \text{8920-bit block codes.}\end{cases} \quad (9)$$

Radio loss as calculated from the above model is plotted in Figures 2, 3, 4 and 5 for residual and suppressed carrier and short and long code blocks. Also shown in those figures are the experimental determinations of radio loss [3] using the simulation method outlined in Appendix A.

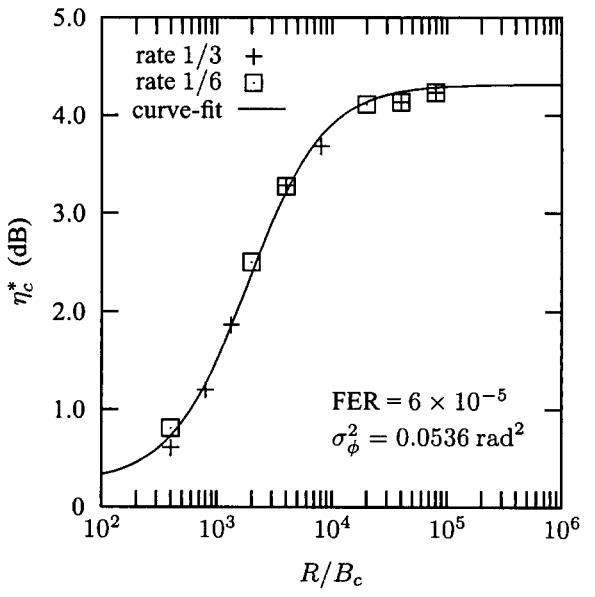

Figure 2: Residual carrier (1784, 1/3 & 1/6)

FER is plotted versus E_b/N_0 in Figures 6 and 7. There is good agreement between the above loss models and the simulation data.

4. Optimizing the Modulation Index for Residual-Carrier BPSK

In residual-carrier operation, it is important to optimize the modulation index. This is shown in Figure 8.

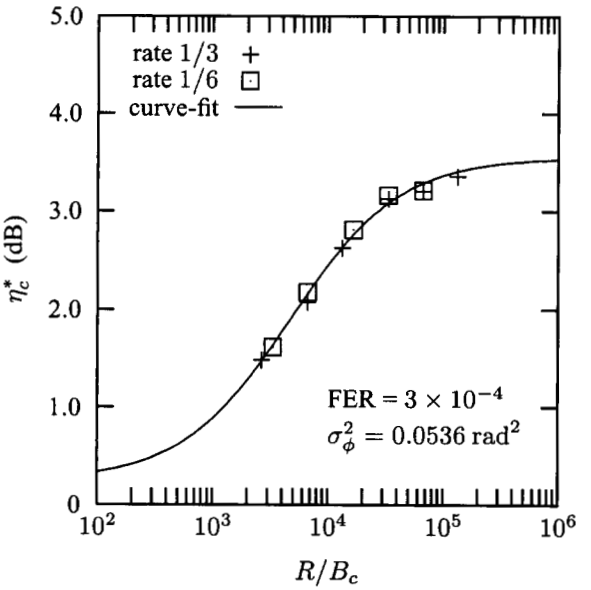

Figure 3: Residual carrier (8920, 1/3 & 1/6)

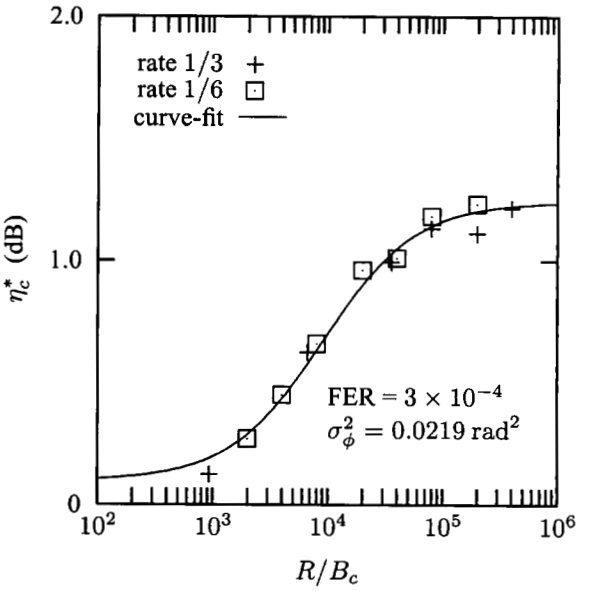

Figure 5: Suppressed carrier (8920, 1/3 & 1/6)

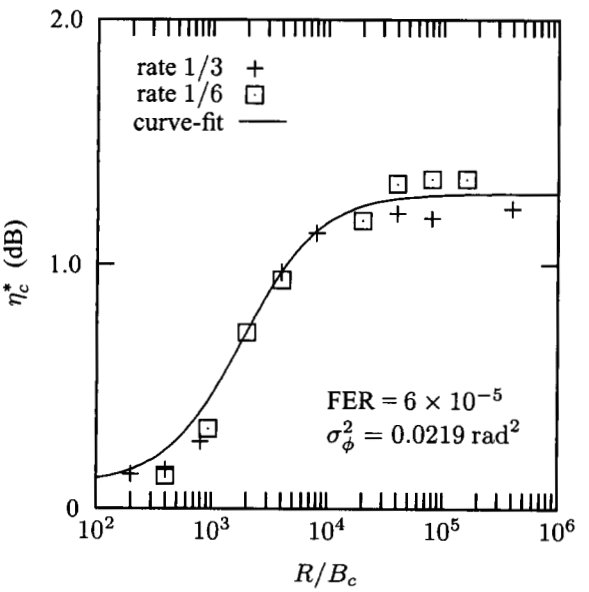

Figure 4: Suppressed carrier (1784, 1/3 & 1/6)

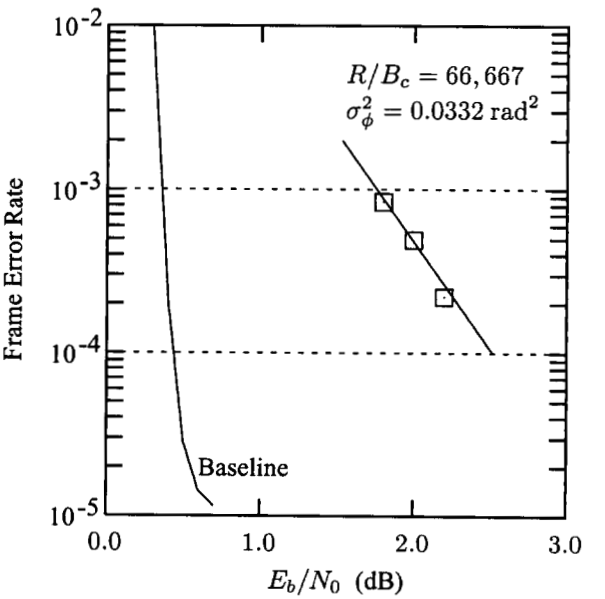

Figure 6: Residual carrier (8920, 1/3)

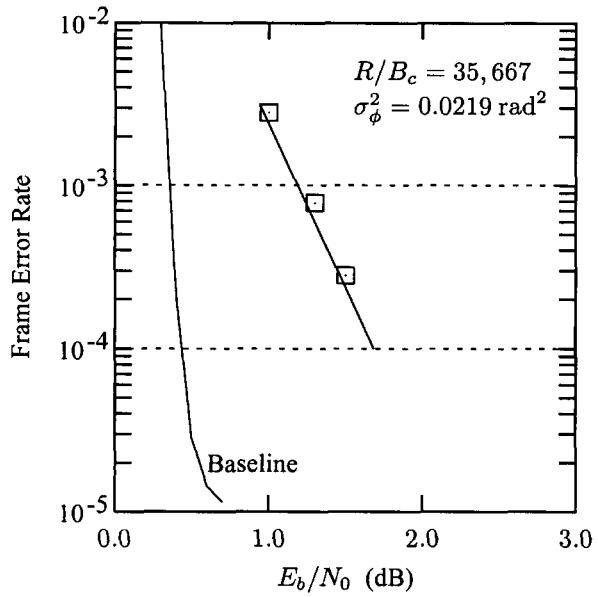

Figure 7: Suppressed carrier (8920, 1/3)

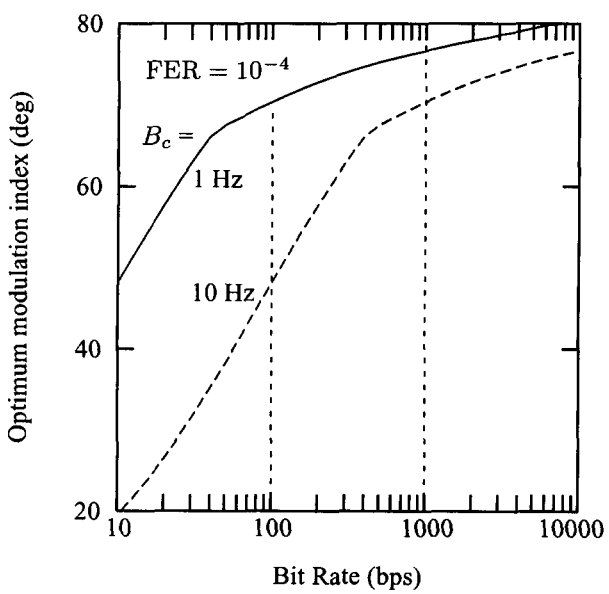

Figure 8: Optimum modulation index (8920, 1/3)

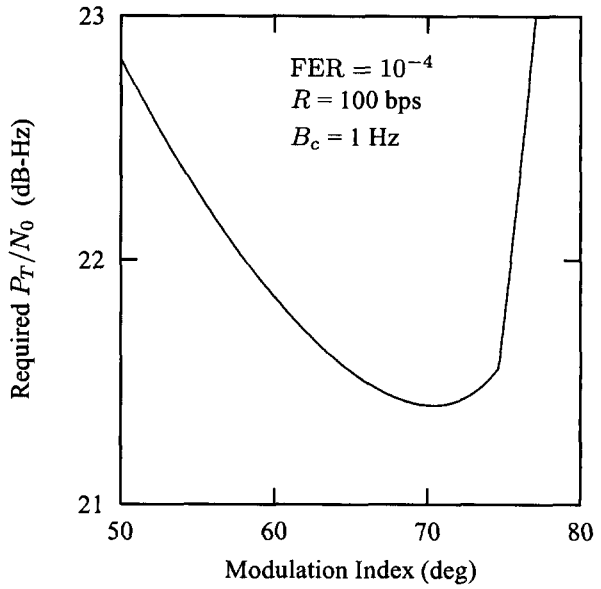

Figure 9: Required P_T/N_0 vs. mod. index (8920, 1/3)

Using the optimum modulation index minimizes the required P_T/N_0. This is shown in Figure 9.

The required P_T/N_0 is a function of bit rate. This is shown in Figure 10. It is clear from this figure that residual-carrier BPSK is to be preferred over suppressed-carrier BPSK for small bit rates.

5. Conclusions

The mathematical models for radio loss given here offer close agreement with simulated data. For residual-carrier BPSK the modulation index may be optimized using these models.

Appendix A: Simulation of Imperfect Carrier Tracking

This Appendix describes how the simulations were done. The simulations were done for both residual-carrier and Costas loops.

The carrier loop phase error is a random process. Realistic samples of this phase error were generated by the method shown in Figure A–1. In that figure $\phi[n]$ is the loop phase error and $\eta_c[n]$ is thermal noise in the carrier loop. (The term $\psi[n]$ could be used to model input phase dynamics, but in these simulations $\psi[n]$ was set to 0.) $g(\cdot)$ is a memoryless, nonlinear function representing the phase detector. $F(z)$ is the loop filter transfer function. $T_u/(z-1)$ represents the numerically-controlled oscillator. T_u is the loop update period (the reciprocal of the loop update rate). The loop phase error samples generated by Figure A–1 (with appropriate statistics for $\eta_c[n]$) have the correct marginal probability density function and the correct correlation among nearby samples.

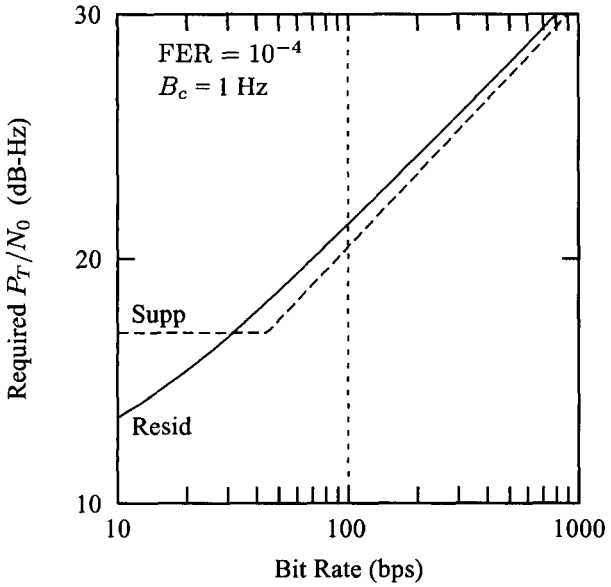

Figure 10: Required P_T/N_0 vs. bit rate (8920, 1/3)

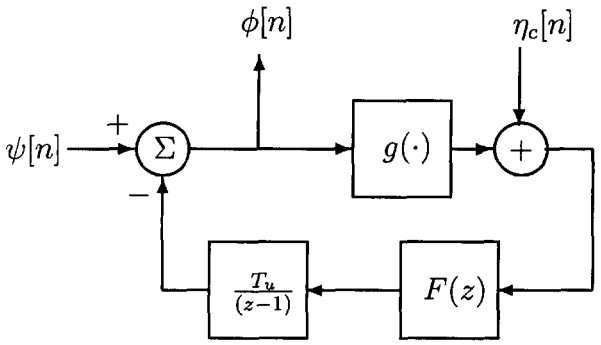

Figure A–1: Loop simulation

The loop filter transfer function is of the form

$$F(z) = \kappa_1 z^{-1} + \kappa_2 \frac{T_u}{z-1}. \tag{A–1}$$

The loop filter coefficients κ_1 and κ_2 are related to the noise-equivalent loop bandwidth B_c by [4]

$$\kappa_1 = \frac{8}{3} B_c, \tag{A–2}$$

$$\kappa_2 = \frac{32}{9} B_c^2. \tag{A–3}$$

Eqs. (A–1), (A–2) and (A–3) are valid for a second-order, standard underdamped loop. Here is the difference equation corresponding to Figure A–1 with $\psi[n] = 0$ and with the $F(z)$ of Eq. (A–1):

$$\begin{aligned} \phi[n] \;=\; & 2\phi[n-1] - \phi[n-2] \\ & -T_u\left(\kappa_1 + \kappa_2 T_u\right)\left\{g\left(\phi[n-2]\right) + \eta_c[n-2]\right\} \\ & +\kappa_1 T_u \left\{g\left(\phi[n-3]\right) + \eta_c[n-3]\right\}. \end{aligned} \tag{A–4}$$

The phase detector function $g(\cdot)$, normalized so that its derivative equals 1 at the origin, is given by

$$g(\phi) = \begin{cases} \sin(\phi), & \text{residual} \\ \frac{1}{2}\sin(2\phi), & \text{suppressed.} \end{cases} \tag{A–5}$$

The noise $\eta_c[n]$ is thermal in origin. $\eta_c[n_1]$ and $\eta_c[n_2]$ are statistically independent for $n_1 \neq n_2$. $\eta_c[n]$ is Gaussian with zero mean and a variance equal to

$$\sigma_c^2 = \begin{cases} \frac{N_0}{2P_c T_u}, & \text{residual} \\ \frac{N_0}{2P_d T_u}\left[1 + \left(2\frac{E_s}{N_0}\right)^{-1}\right], & \text{suppressed,} \end{cases} \tag{A–6}$$

where N_0 is the one-sided thermal noise spectral density. For a residual carrier loop, P_c is the power of the residual carrier. For a Costas loop tracking a suppressed carrier, P_d is the power in the data sidebands.

In all simulations the loop update rate ($1/T_u$) was less than the telemetry symbol rate, so a "re-sampling" was necessary in order to have a common sampling rate for the simulation of telemetry performance. A re-sampling was effected by using each sample of loop phase error multiple times. In the remainder of this appendix a different integer time index (m, rather than n) is used as a reminder of the re-sampling.

The effect of loop phase error on telemetry symbol detection was simulated as described here. Denoting the antipodal telemetry symbols by $d[m]$ ($d[m] = \pm 1$), the effect of loop phase error was modeled as $d[m] \cdot \cos(\phi[m])$. To this was added $\eta_d[m]$, representing the baseband noise of the data channel. The noise samples $\eta_d[m]$ are zero mean and Gaussian, with uncorrelated successive samples, and with a variance equal to

$$\sigma_d^2 = \frac{N_0}{2P_d T_s}, \tag{A–7}$$

where T_s is the symbol period. The symbol period is related to the bit rate R through

$$T_s = \begin{cases} \frac{1}{3R}, & \text{rate } 1/3 \text{ code} \\ \frac{1}{6R}, & \text{rate } 1/6 \text{ code.} \end{cases} \tag{A–8}$$

The input to the software turbo decoder was

$$d[m] \cdot \cos(\phi[m]) + \eta_d[m],$$

represented as a floating-point number.

Appendix B: Low-Rate and High-Rate Models

Imperfect carrier tracking causes a (random) fractional factor $\cos\phi$ to multiply the baseband signal at the output of the phase detector. The baseband signal is averaged over one symbol period T_s by the matched filter. The carrier loop phase error ϕ is a random process. When ϕ changes quickly compared with the telemetry symbol rate, so that the average of $\cos\phi$ over a time period T_s fairly represents the average of $\cos\phi$ over *all* time, then the *low-rate model* (LRM) accurately predicts radio loss. (The name of this model comes from the fact that the symbol rate is low compared with the bandwidth of the process ϕ.) The conditions that make the LRM valid seldom occur in practice. Nonetheless, this model is still useful as an asymptote of performance. When, on the other hand, ϕ changes slowly compared with the duration of a code block of telemetry, the *high-rate model* (HRM) applies. Both of these models, which have long been available [5], are summarized in this appendix.

Both models are based on the assumption that the marginal probability density function of ϕ is Tikhonov [6],

$$p_\phi(\phi') = \begin{cases} \frac{e^{\rho\cos\phi'}}{2\pi I_0(\rho)}, & \text{residual} \\ \frac{e^{(\rho/4)\cos\phi'}}{2\pi I_0(\rho/4)}, & \text{suppressed,} \end{cases} \tag{B–1}$$

where $I_0(\cdot)$ is the modified Bessel function of the first kind of order zero. Figure B–1 shows the Tikhonov probability density function (solid curve) for residual-carrier tracking with a carrier loop signal-to-noise ratio $\rho = 10$. An experimental distribution of ϕ was obtained using the loop simulation described in Appendix A; this experimental distribution also is shown in Figure B–1. (The simulation was done with a carrier loop bandwidth B_c of 10 Hz, a loop update rate of 2000 Hz, and a ρ of 10.) As the figure clearly shows, the Tikhonov probability density function accurately models the distribution of ϕ.

Low-Rate Model

The LRM radio loss is

$$\begin{aligned} L_{LRM} &= \left(\mathrm{E}\{\cos\phi\}\right)^{-2} \\ &= \begin{cases} \left[\frac{I_0(\rho)}{I_1(\rho)}\right]^2, & \text{residual} \\ \left[\frac{I_0(\rho/4)}{I_1(\rho/4)}\right]^2, & \text{suppressed,} \end{cases} \end{aligned} \tag{B–2}$$

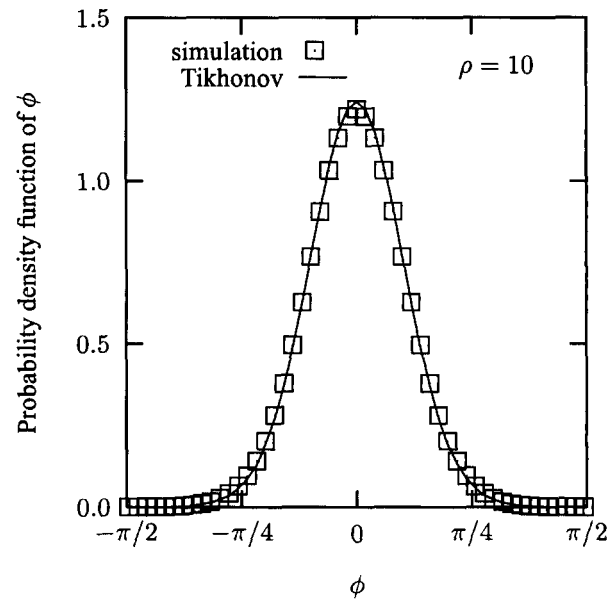

Figure B–1: Tikhonov density function

where $I_1(\cdot)$ is the modified Bessel function of the first kind of order one. L_{LRM} is greater than 1 and so has a positive number of decibels that diminish the effective E_b/N_0, as indicated in Eq. (5). L_{LRM} is a function of ρ, and it also depends on whether the tracking is done by a residual-carrier loop or a Costas loop; it is independent of the code and the threshold FER.

High-Rate Model

The HRM is based on the assumption that ϕ is unvarying during an entire code block of telemetry. This condition is only met for very high bit rates. The HRM is a useful asymptote of performance, even when the high-rate condition is not met. Because ϕ is unchanging during a code block in this model, the factor $\cos\phi$ is not affected by the averaging of the matched filter. The bit energy to noise spectral density ratio for any given code block is diminished by a factor $\cos^2\phi$. Different code blocks will, in general, experience different factors $\cos^2\phi$. The average FER is given by

$$\mathrm{FER} = \int_{-\pi/2}^{\pi/2} f\left(\frac{E_b}{N_0}\cos^2\phi'\right) p_\phi(\phi')\, d\phi', \tag{B–3}$$

where $p_\phi(\phi')$ is the Tikhonov probability density function of Eq. (B–1). The integral of Eq. (B–3) ignores the possibility that ϕ could be outside the bounds $|\phi| \le \pi/2$. A more general theory would consider such outlying values for ϕ and the probability of their occurrence. But for $\rho \ge 10$, these outlying values occur with such low probability that it is legitimate to neglect them.

The HRM radio loss L_{HRM} is evaluated by first finding the E_b/N_0 that satisfies Eq. (B–3) for the threshold FER. Then this E_b/N_0 is converted to decibels and substituted into the

following equation:

$$L_{HRM}\,(\text{dB}) = \frac{E_b}{N_0}\,(\text{dB}) - \left.\frac{E_b}{N_0}\right|_{\text{base}}\,(\text{dB}). \qquad \text{(B–4)}$$

The result is always a positive number of decibels for L_{HRM}. All of the following affect L_{HRM}: the code, the threshold FER, ρ, and the type of tracking loop.

ACKNOWLEDGMENT

The research described in this paper was carried out at the Jet Propulsion Laboratory, California Institute of Technology, under a contract with the National Aeronautics and Space Administration.

REFERENCES

[1] K. Andrews, V. Stanton, S. Dolinar, V. Chen, J. Berner, and F. Pollara, "Turbo-Decoder Implementation for the Deep Space Network," *The Interplanetary Network Progress Report 42–148*, February 15, 2002. *http://tmo.jpl.nasa.gov/progress_report/*

[2] *DSMS Telecommunications Link Design Handbook*, JPL Doc. 810–005, Jet Propulsion Laboratory, Pasadena, CA. *http://eis.jpl.nasa.gov/deepspace/dsndocs/810-005/*

[3] S. Shambayati, L. Tadjpour, and P. Kinman, "Turbo Code Carrier Synchronization Losses (Radio Losses)," *AIAA 19th Int. Communications Satellite Systems Conference and Exhibit*, Toulouse, France, April 17-20, 2001.

[4] S. A. Stephens and J. B. Thomas, "Controlled-Root Formulation for Digital Phase-Locked Loops," *IEEE Trans. on Aerospace and Electronic Systems*, Vol. 31, No. 1, pp. 78–95, January 1995.

[5] J. H. Yuen, ed., *Deep Space Telecommunications Systems Engineering*, Plenum Press, New York, 1983.

[6] A. J. Viterbi, *Principles of Coherent Communication*, McGraw-Hill, New York, 1966.

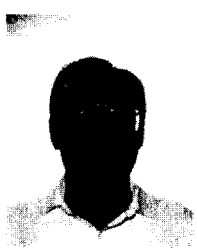

Peter W. Kinman (S'73, M'79, SM'91) was born in Saint Louis, Missouri, in 1955. He received B.S. degrees in Electrical Engineering and Physics from the University of Missouri–Rolla and a Ph.D. in Electrical Engineering from the University of Southern California. He was employed by the Jet Propulsion Laboratory from 1979 to 1993, where he worked on telemetry and Doppler and range measurements in support of deep space exploration. Since 1993 he has been a researcher at Case Western Reserve University, specializing in radio technology for space communications.

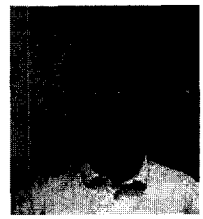

Shervin Shambayati obtained his Bachelors of Science degree in Applied Mathematics and Engineering in 1989 from California State University, Northridge. Subsequently, he obtained his MSEE, Engineer's Degree and Ph.D. from University of California, Los Angeles in 1991, 1993 and 2002, respectively. In 1993, Dr. Shambayati joined Deep Space Communications Systems Group at Jet Propulsion Laboratory where he took part in development and testing of Deep Space Network's Galileo Telemetry receiver (DGT). In 1997, Dr. Shambayati joined the Information Processing Group at JPL where he has been working ever since. With that group Dr. Shambayati has been involved in various projects including Mars Global Surveyor's Ka-Band Link Experiment II, Deep Space 1 Ka-band testing and 70m antenna Ka-band Task. Dr. Shambayati's current research interests and activities include evaluating the effects of weather outage on the spacecraft resources, Ka-band weather forecasting, Ka-band link design for Mars Reconnaissance Orbiter and Mars Telecommunication Satellite and engineering support for implementation of Ka-band services in NASA's Deep Space Network.

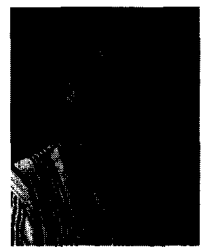

Jeff B. Berner (S'82, M'84, SM'98) earned his B.S. (with honors) in Electrical Engineering in 1983 and his M.S. in Electrical Engineering in 1984, both from the California Institute of Technology. With the exception of a six-month period in 1984, he has been at the Jet Propulsion Laboratory since 1982. Early in his career, he worked on projects such as the Galileo and Mars Observer spacecraft, and the Mobile Satellite Experiment (MSAT-X). More recently, he was the Cognizant Development Engineer of the Block V Receiver, the tracking and telemetry receiver of the Deep Space Network. In 1996, he was awarded the NASA Exceptional Service Medal for his work with the Block V Receiver for the Galileo project. Currently, he is the Telecommunications and Mission Operations Directorate Telecommunications Services System Development Engineer, where he is responsible for the uplink, downlink, and tracking equipment design and performance, and for the Spacecraft Transponding Modem signal processing architectural design.